



# Mangrove Species Discrimination from Very High Resolution Imagery Using Gaussian Markov Random Field Model

Luoma Wan<sup>1</sup> · Hongsheng Zhang<sup>1,2</sup> · Ting Wang<sup>1,3</sup> · Gang Li<sup>1</sup> · Hui Lin<sup>1,2,4,5</sup>

Received: 21 April 2017 / Accepted: 2 June 2017 / Published online: 18 September 2018  
© Society of Wetland Scientists 2018

**Abstract** Mangrove forests are the most productive ecosystem for tropical and subtropical flora, but they are experiencing serious loss. Urgent measures should be taken for conservation and restoration, including investigation of mangrove species constitution using satellite imagery in which texture provides effective information. However, differentiation by texture for various species of mangroves is underexplored. The Gray Level Co-occurrence Matrix (GLCM) has proved to be a common approach to describing texture in most previous studies, while other textural measurements such as the Gaussian Markov Random Field (GMRF) have seldom been tested and applied. This study aimed to provide a comprehensive assessment and comparison of textures using GLCM and GMRF to offer a better understanding of their roles in mangrove species discrimination using very high-resolution satellite data. The experiments were designed to highlight two aspects of textural features - local pattern and textured region size - to assess their effect on mangrove species discrimination based on texture definition. The results indicated that

adjusting the textured region size can easily improve texture extraction, and GMRF outperformed GLCM in texture representation of mangrove forest using the same parameters, with an increase in overall accuracy (1.54%, 6.47% and 10.66% on average at three different local pattern sizes).

**Keywords** Gaussian Markov random field · Mangrove species discrimination · Texture

## Introduction

Mangrove forests are the most productive ecosystems for tropical and subtropical flora and play an essential role in environmental protection through activities such as preventing soil erosion and loss and conserving plant biodiversity. Approximately 20 % of global mangrove forests were lost from 1980 to 2005 (NC 2005), which has provoked concern about dynamic mangrove monitoring and protection among government officials and scientists. Information about the important characteristics of mangrove forest such as species constitution is valuable for the sustainable management of mangrove forests and invasive species monitoring (Heumann 2011). Some species, including *Pelliciera rhizophorae*, have become vulnerable and endangered (Ellison et al. 2010).

Conventional satellite imagery with spatial resolution ranging from 100 m to 30 m has been widely used to separate mangrove from non-mangrove habitats, but it is not appropriate for mangrove species discrimination because different mangrove species were depicted within a small patch size of a coarse-resolution image (Jia et al. 2014; Wang et al. 2004a). Although some researchers have succeeded in mangrove species discrimination using hyperspectral imagery, Wang et al. (2004b) noted that resolution increments in space might be more efficient than that of the spectra for mangrove

✉ Hongsheng Zhang  
zhangstream@gmail.com

<sup>1</sup> Institute of Space and Earth Information Science, The Chinese University of Hong Kong, Shatin, New Territories, Hong Kong

<sup>2</sup> Shenzhen Research Institute, The Chinese University of Hong Kong, Shenzhen, China

<sup>3</sup> Hubei Bureau of Surveying, Mapping and Geoinformation, Wuhan, China

<sup>4</sup> Department of Geography and Resource Management, The Chinese University of Hong Kong, Shatin, New Territories, Hong Kong

<sup>5</sup> Key Laboratory of Poyang Lake Wetland and Watershed Research, Ministry of Education, Jiangxi Normal University, Nanchang 330022, China

species discrimination of some mangrove species at small patch sizes. Very high resolution (VHR) imagery with (sub)meter resolution provides more detailed spatial information, making it possible to discriminate between mangroves at the species level.

Texture reveals information about spatial distribution by building a relationship between the pixels within a region (Tuceryan and Jain 1993; Zhang et al. 2013). As a complement to spectral features, texture can significantly improve classification accuracy, especially for images with detailed structures (Feng et al. 2015; Wang et al. 2015; Pham et al. 2016). During the past decades, research has explored the potential use of texture in VHR images for mangrove species discrimination. Using IKONOS and QuickBird (Wang et al. 2004b), second-order texture features have been substituted for costly airborne images for use in mangrove species discrimination (Sulong et al. 2002; Verheyden et al. 2002). Neukermans et al. (2008) further investigated the potential of QuickBird satellite images in the visual interpretation of mangrove stand discrimination with texture in Gazi Bay. Effective use of IKONOS satellite images for discrimination between two mangrove species within the same genus was also reported in Sri Lanka (Dahdouh-Guebas et al. 2004). Recently, textured WorldView 3 satellite images were introduced as a source material for mangrove species discrimination in Hong Kong (Wang et al. 2015).

Nevertheless, few texture extraction methods have been utilized for texture analysis in mangrove species discrimination. Though lacunarity has been characterized as an identifying texture for mangrove species (Myint et al. 2008), it has largely been employed to identify land use for three species using Landsat Thematic Mapper images. Morphological texture was investigated for use in discriminating between three mangrove species on the Caribbean coast of Panama and with multispectral IKONOS imagery performed at higher accuracy than GLCM textures (89.1% versus 81.9%) (Huang et al. 2009). Beyond that, GLCM texture has been the default choice for texture analysis in mangrove species discrimination using VHR imagery. Meanwhile, there has been no exhaustive test of various texture methods to determine whether higher spatial resolution corresponds to better texture-based discrimination in mangrove species (Wang et al. 2004b).

Bharati et al. (2004) divided the various texture methods into four categories: statistical methods, structural methods, model-based methods, and transform-based methods. GLCM is one of the statistical methods. The selection of texture methods varies with the type of texture. For stochastic texture images, such as satellite images of mangrove forest, structural methods are inappropriate due to the difficulties in extracting the primitive texture (Gonzalez and Woods 1992). Transform-based methods such as wavelet and Gabor are also excluded in this study because they process in the frequency domain. Model-based methods model texture as a stochastic process, and textured images are viewed as a realization or as samples from parametric probability

distributions on the image space (Cohen et al. 1991a). The notable advantage of this method is the capability to produce textures which match the observed textures, even stochastic textures. A classic model-based method, Gaussian Markov random field (GMRF), has been used to describe texture in various applications (Çesmeli and Wang 2001; Xia et al. 2006). However, little work has been done to apply GMRF to VHR satellite images for mangrove species discrimination.

In this study, GMRF was applied to mangrove species discrimination using VHR satellite imagery to provide a deeper understanding of texture and more choices for texture utilization. First, the study area and data sets were introduced. Then, GMRF was analyzed from two aspects based on texture definition and compared to GLCM. Furthermore, the results and discussion were provided in **Results and Discussion** section. Finally, the study concluded with some findings and limitations.

## Study Area and Data Sets

### Study Site

Mai Po Marshes Nature Reserve (MPMNR, Fig. 1b) ( $113^{\circ}59' E - 114^{\circ}3'E$ ,  $22^{\circ}28'N - 22^{\circ}32'N$ ) is located in the northwest region of the New Territories, on the shores of Deep Bay Wilkie and Fortuna (2003). The mangrove forest located there is the largest ( $1.7 km^2$ ) in Hong Kong and surrounded by shrimp/fish ponds, reed beds and an extensive area of intertidal mudflats (Zheng et al. 2000). The reserve is divided by the Agriculture, Fisheries and Conservation Department (AFCD) of Hong Kong into the core zone, the biodiversity management zone, the wise use zone, the public access zone and the private land zone according to their function. Mangroves largely occupy the core zone with partial distribution in other zones (Qin et al. 2000).

Eight species of mangroves have been reported in this area (AFCD 2015). However, only four dominant species including *Avicennia marina* (AM), *Acanthus ilicifolius* (AI), *Kandelia obovata* (KO), and *Aegiceras corniculatum* (AC) were found during our fieldwork (Wang et al. 2015). As AI has leaves with serrated or rounded edges and KO located landward and seaward have different tree heights and leaf densities, each species is further separated into two sub-classes, AI group 1 (AII), AI group 2 (AI2) and KO group 1 (KO1), KO group 2 (KO2) (Wong and Fung 2014; Wang et al. 2015). *Sonneratia apetala* and *Sonneratia caseolaris* float into the reserve from the Futian National Nature Reserve of Shenzhen, and due to their high adaptability and threat of potential colonization, these two species are viewed as invasive species and have been consistently removed by the government of Hong Kong (AFCD) to protect native species (Peng 2003; Ren et al. 2009; Wong and Fung 2014). Therefore, six mangrove species were considered in the study: AM, AII, AI2, KO1, KO2, and AC.

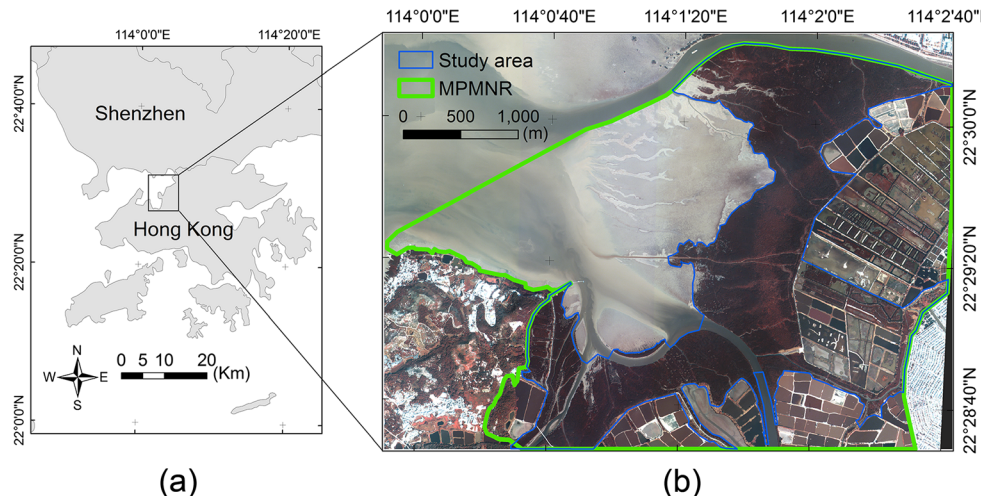


**Fig. 1** Location of the Mai Po Marshes Nature Reserve, Hong Kong (a) and a false color (321) WorldView-3 image of Mai Po Marshes Nature Reserve (b)

## Satellite Data and Pre-Processing

WorldView-3 (WV3) provides 0.4 m panchromatic resolution, 1.6 m multispectral resolution including four standard visible and near infrared (VNIR) bands, and four added VNIR bands (Table 1) (Globe 2014). WV3 images have been applied in various fields, such as mineral mapping (Kruse and Perry 2013), hydrocarbons detection (Asadzadeh and de Souza Filho 2016), urban tree species mapping (Li et al. 2015), and mangrove species discrimination (Wang et al. 2015), etc.

A WV3 standard image (level 2, Fig. 1b) covering the majority region of MPMNR was acquired on January 26, 2015. It was delivered in a georegistered UTM/WGS84 projection with an 11-bit depth standard ENVI format with basic preprocessing including radiation correction, sensor correction and geometrical correction, resulting in eight resampled multispectral bands with a 1.6-m spatial resolution.

To discriminate between mangrove species, other cover types such as water, bare soil and urban area should be excluded. The original image was first classified based on the spectral difference using support vector machine, and the isolated pixels occurring in the classification image were removed via “sieve classes” and “clump classes” with a

minimal number of 4 and a neighborhood size of 8 in ENVI. The boundary of MPMNR and its core zone was also assisted in depicting the mangrove region. Furthermore, visual interpretation at the panchromatic band and in previous fieldwork was utilized to refine the mangrove area (Fig. 1). To enlarge the experimental data, several regions outside of the core zone were also included.

The field survey was conducted on November 10, 2015. Due to the strict protection of mangrove forest and limited access policy, collecting reference data in MPMNR is extremely difficult. Using visual interpretation over the multispectral (1.6 m) and panchromatic (0.4 m) WV3 data, 942 reference samples in total and 11 classes (6 mangrove species and 5 other classes, Table 2) were collected, in which 80% were randomly selected as the training set and the rest used for validation.

## Methods

### Gaussian Markov Random Field (GMRF) Model

Texture is defined as a function of the spatial variation in the pixel intensities of an image and reveals information on the distribution and the relationship of the pixels within a region (Tuceryan and Jain 1993). To deduce this function, a small region (referred to as “neighborhood” in some literature) is determined to define the homogeneous pixels presenting the local information and thereafter referred to as “local pattern.” Generally, the local pattern describes a part of a meaningful object. To describe the complete object or a minimal unit distinguished from other objects, a large region (referred to as “textured region” (Hawkins 1970)) is needed to include sufficient local patterns. The relationship between these local patterns is further formulated by a function with many parameters or indices, which are used as texture features. The relationship between neighborhood and textured region is shown in Fig. 2.

**Table 1** Eight multispectral bands of WorldView 3

| BAND     | SPECTRA (nm) |
|----------|--------------|
| Blue     | 450–510      |
| Green    | 510–580      |
| Red      | 630–690      |
| Near-IR1 | 770–895      |
| Coastal  | 400–450      |
| Yellow   | 585–625      |
| Red-edge | 705–745      |
| Near-IR2 | 860–1040     |

**Table 2** Samples for training and validation

| CLASS            | NUMBER |
|------------------|--------|
| AM               | 80     |
| AI2              | 57     |
| KO2              | 64     |
| Other Vegetation | 82     |
| Mudflats         | 180    |
| Bare soil        | 39     |
| AII              | 80     |
| KOI              | 100    |
| AC               | 35     |
| Water            | 148    |
| Urban            | 77     |

Mudflats provide a hospitable environment for mangrove forest growth, while bare soil refers to land with exposed soil, sand, or rocks and has less than 10% vegetated cover during any time of the year

A random field is a set of random variables defined on the set  $S$ . It is a Markov random field (MRF) on  $S$  with respect to a neighborhood system  $N$  if and only if the joint probability that the random variable takes any value on the set is positive and the conditional probabilities of a random variable given the rest of the random variables is determined by the random variables in its neighborhood (Li, S. Z. 2009). The properties of the conditional probabilities depict the local characteristics of the random field.

An MRF is specified by defining the conditional probabilities or the joint probability. The probability determines how likely a texture pattern is to occur. The Hammersley-Clifford theorem (Hammersley and Clifford 1971) proves that a Gibbs distribution (GRF) is an MRF and provides a simple way to specify the joint probability by defining the potential functional forms and estimating the parameters. In MRF-based texture modeling, a texture is assumed to be an MRF, texture features correspond to the MRF texture parameters and feature extraction is equivalent to parameter estimation.

Gaussian MRF (GMRF) is an auto-normal model where the set is the real line and the joint distribution is multivariate normal. It is a stationary non-causal two-dimensional autoregressive process (Cohen et al. 1991b; Cao et al. 2006) and conveys the contextual information using contextual

constraints on two sites. In a stochastic representation, an image can be viewed as a sample function of a random field. The intensity  $I(x, y)$  of an image at pixel  $(x, y)$  can be formulated using the following difference equation,

$$I(x, y) = \sum_{(\Delta_x, \Delta_y)} (I(x + \Delta_x, y + \Delta_y) + I(x - \Delta_x, y - \Delta_y)) + e(x, y), \\ (x \pm \Delta_x, y \pm \Delta_y) \in N_{(x, y)} \quad (1)$$

where  $N$  is a symmetric neighbor set and  $e(x, y)$  is the zero-mean stationary Gaussian noise sequence with the following properties.

$$E(e(x, y)I(x', y')) = \begin{cases} 0, & (x, y) \neq (x', y') \\ v, & (x, y) = (x', y') \end{cases} \quad (2)$$

Therefore, the GMRF is parameterized by the unknown parameters  $\theta_{(\Delta_x, \Delta_y)}$  and  $v$ , which can be estimated using the least squares (LS) method as shown below (Chellappa and Chatterjee 1985). These are commonly used as the texture descriptors.

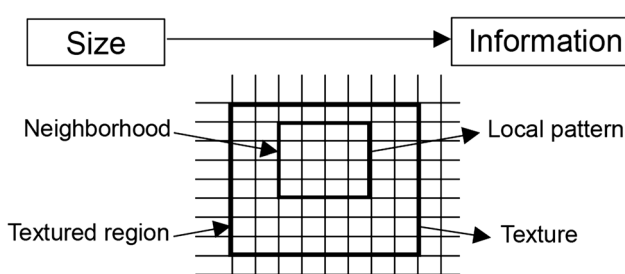
$$\theta^* = [\sum q(x, y)q'(x, y)]^{-1} [\sum q(x, y)I(x, y)] \quad (3)$$

$$v^* = \frac{\sum [I(x, y) - \theta^* q(x, y)]^2}{M^2} \quad (4)$$

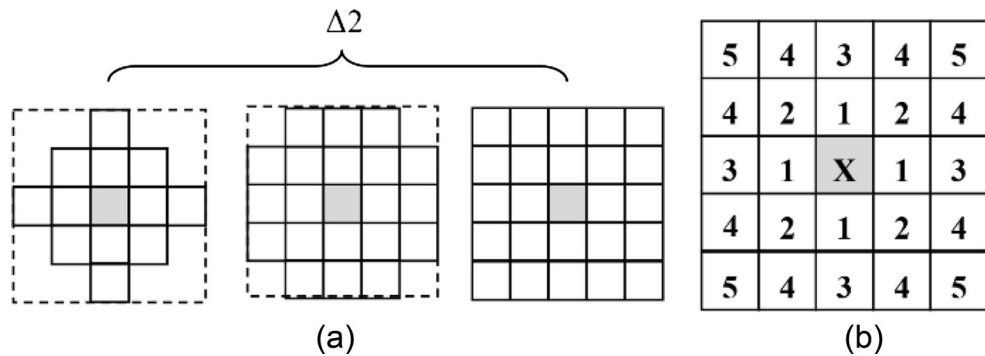
where  $q(x, y) = \text{col}[I(x + \Delta_x, y + \Delta_y) + I(x - \Delta_x, y - \Delta_y)]$ ,  $(x \pm \Delta_x, y \pm \Delta_y) \in N_{(x, y)}$ . The offset  $(\Delta_x, \Delta_y)$  is usually set to some certain values ( $\Delta_1, \Delta_2, \Delta_3$ , see Eq. (5)), and its maximum value is less than or equal to three because of the intensive cost with little improvement in performance incurred by the increase in dimensions. Importantly, there is more than one order for an offset. The offset of  $\Delta_2$ , for instance, has three orders (Fig. 3a). The order of GMRF can also be seen in detail in Fig. 3b.

$$\begin{aligned} \Delta_1 &= \{\Delta_x, \Delta_y\} = \{(0, 1), (1, 0), (1, 1), (1, -1)\} \\ \Delta_2 &= \{\Delta_1, (0, 2), (1, 2), (1, -2), (2, 0), (2, 1), \\ &\quad (2, -1), (2, 2), (2, -2)\} \\ \Delta_3 &= \{\Delta_1, \Delta_2, (0, 3), (1, 3), (1, -3), (2, 3), (2, -3), \\ &\quad (3, 1), (3, -1), (3, 2), (3, -2), (3, 3), (3, -3)\} \end{aligned} \quad (5)$$

It is apparent that the offset qualifies the neighborhood of GMRF and the order together with the central pixel qualifies which pixels in the neighborhood will be used to describe the local pattern. The size of the local pattern is the neighborhood size. A local pattern of GMRF is a different equation (Eq. (1)), in which the number of parameters is determined by the order. The parameters can only be estimated where the number of difference equations is greater than the number of parameters. Therefore, for GMRF to cover sufficient local patterns, a larger textured region is needed.

**Fig. 2** The relationship between neighborhood and textured region

**Fig. 3** Three modes of GMRF with neighborhood size of 5 (a) and the neighborhood of GMRF (b), in which the numbers indicate the order of the model relative to x



### Comparison and Assessment of the GMRF Model

Gray Level Co-occurrence Matrix (GLCM) (Haralick and Shanmugam 1974; Haralick 1979) is widely used to describe texture. Using GLCM, the local pattern is reflected in the change intensity of the pixel pairs. Therefore, the distance (offset) and the direction specifying the pixel pairs determines the local pattern. Additionally, the textured region assumed to be homogeneous is also specified to count the number of local patterns which forms the co-occurrence matrix. Four texture measures including contrast, correlation, homogeneity and entropy derived from the co-occurrence matrix (Haralick et al. 1973) were employed for comparison. The major differences between GMRF and GLCM are as follows:

- 1) One more step of quantizing the gray level is operated before executing GLCM. Given that the quantization leads to information loss and texture change, it was excluded in this study.
- 2) For GLCM, the average of four features in different directions ( $0^\circ$ ,  $45^\circ$ ,  $90^\circ$ , and  $135^\circ$ ) was suggested to avoid angular effect (Haralick et al. 1973), while the directionality is embedded in the parameter  $\theta$  (usually more than four parameters) of GMRF. More directions increase the potential to describe complex texture.
- 3) The pixels used to describe the local pattern of GLCM distribute on the margin of the neighborhood, while those pixels distribute in the whole neighborhood for GMRFs. More pixels lead to more detailed information.
- 4) Two steps including co-occurrence matrix formation and texture indices calculation are involved in GLCM, while one step, namely, parameter estimation, is utilized to obtain the GMRF features. This means that the GMRF features can be extracted by simply fitting the model to a texture pattern (Chen and Huang 1993).

However, the similarity between GLCM and GMRF is that the local pattern (offset for GLCM and order for GMRF) and the size of the textured region are the factors which influence texture features.

### Mangrove Species Discrimination and Accuracy Assessment

After extracting texture from the original spectral image (OSI) using GMRF and GLCM, we obtained many texture feature images with the same size as that of the original image. Furthermore, these texture feature images were stacked on the original spectral image bands to form a multi-band features image, which were input to the classifier. Combined with the texture derived from GMRF and GLCM, the original spectral image can form two multi-band features images named OGMRF and OGLCM, respectively.

Support vector machine (SVM) is a machine learning algorithm used to find a maximum-margin hyperplane in parameters space and maximize the margin between the separating hyperplane and the data with the minimal error (Boser et al. 1992; Cortes and Vapnik 1995). It has been widely used for classification of multispectral remote sensing images (Roli and Fumera 2001; Huang et al. 2002) due to a larger number of classification accuracy provisions than other techniques, such as maximum likelihood. Additional principles were also taken into consideration when applying SVM to mangrove species discrimination:

- 1) High dimensional features (of 200 at most) are obtained when combining spectrum and texture features. SVM can analyze hyper-dimensional features effectively without any feature-reduction procedures (Melgani and Bruzzone 2004; Huang and Zhang 2013). It maintains high computing performance and easy usage.
- 2) A limited number of training samples (334 in total for mangroves of 6 classes) is available in this study. SVM is insensitive to the number of training samples, showing a notable advantage in classifying heterogeneous classes for which only few training samples are available (Melgani and Bruzzone 2004).
- 3) SVM can be conducted without a required estimation of class distribution (Huang and Zhang 2013).

In SVM applications, the selection of kernel functions is critical (Mountrakis et al. 2011). To date, no data-

dependent theories about kernel functions selection have been proposed (Amari and Wu 1999). Generally, linear and radial basis function (RBF) are recommended to address linearly separable and non-separable problems. In this study, RBF was chosen as a linear function is a special case of RBF (Keerthi and Lin 2003). Consequently, a penalty parameter (usually denoted by  $C$ ) and an RBF width parameter (usually denoted by  $\gamma$ ) are considered in this study. Finally, cross-validation (Hsu et al. 2003), a common strategy, was adopted to search for an optimal  $C$  and  $\gamma$ , and this procedure was completed via the LibSVM tool (Chang and Lin 2011).

For validation, the confusion (or error) matrix (Mather and Tso 2003) usually used for classification accuracy assessment was adopted. Furthermore, overall accuracy and the kappa coefficient (Cohen 1960; Congalton 1983) were derived from the confusion matrix to indicate classification accuracy.

Since both GMRF and GLCM textures vary with the local pattern and the textured region size, their influences on mangrove species discrimination were first analyzed individually. This also provided useful information about parameters selection for the subsequent procedure – the comparison between GMRF and GLCM of mangrove species discrimination using texture. The result with spectral information only was also added as a benchmark. The whole procedure is illustrated in Fig. 4.

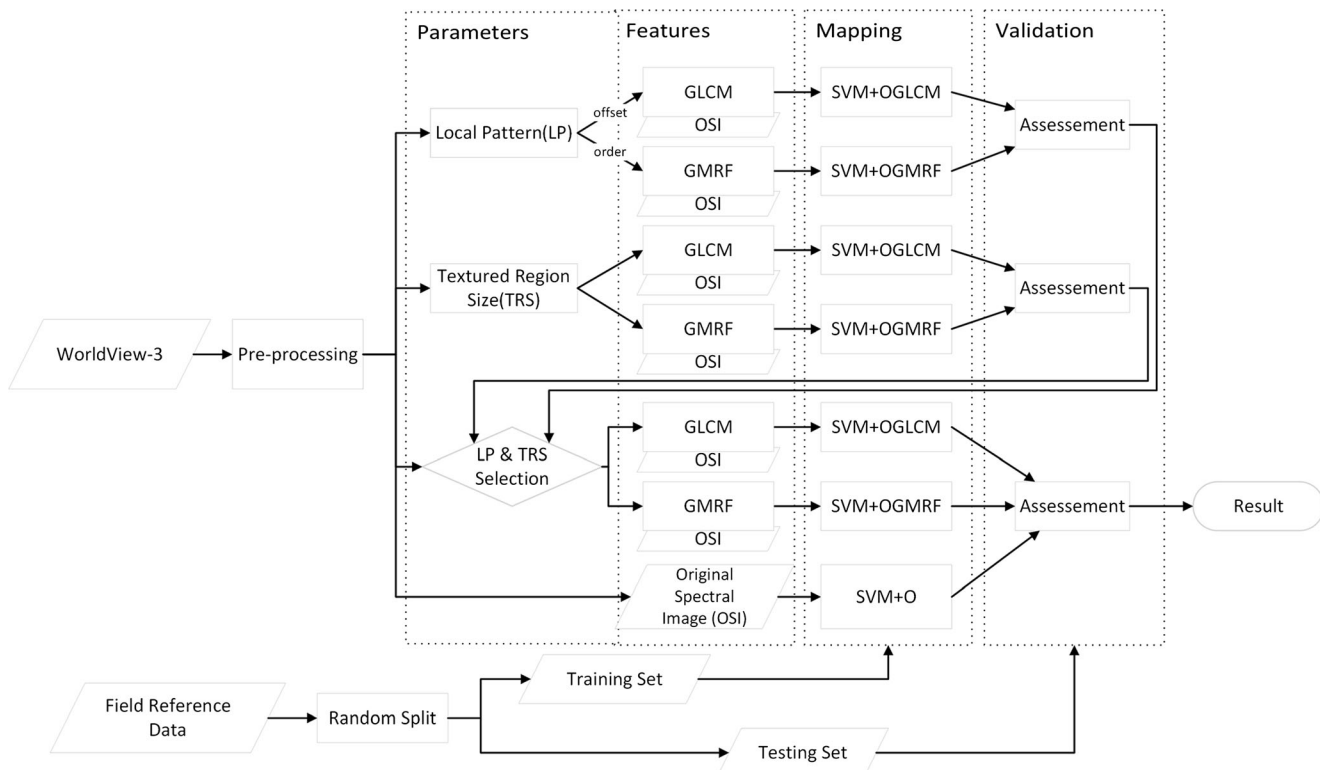


**Fig. 4** Methods flowchart

## Results and Discussion

### The Effect of Local Pattern on Mangrove Species Discrimination

Fixing textured region size, the offset of GLCM varies from 1 to 7 to extract texture features. A 4-band texture image can be derived from each band and a final OGLCM image with 40-band ( $8 + 8 \times 4 = 40$ ) can be obtained. This procedure is repeated with different textured region sizes ( $S_{tr} = 9, 11, 13, \dots, 35$ ). Similarly, the whole process can be replicated using GMRF with orders from 2 to 9 at 16 textured region sizes ( $S_{tr} = 7, 9, \dots, 35$ ). The difference between GMRF and GLCM is that the dimension of the OGMRF image varies with the order (Table 3).

Based on the location of the reference samples, we can obtain a feature vector for each sample from the OGLCM or OGMRF. After applying SVM to feature vectors of training samples and classifying the OGLCM or OGMRF image via the SVM model trained in the previous step, the overall accuracy is finally calculated based on the testing samples (Fig. 5). Generally, there is no significant change in horizontal direction, while the change in vertical direction is greater. To demonstrate the trend clearly, a trend line for each change was calculated and the slope was used as the indicator for trend (Fig. 5c). The negative value for the slope of GLCM indicates that the

**Table 3** The dimensions of texture feature vector extraction from a one-dimensional image using GMRF

| Ns*   | 3     | 5       | 5       | 5        | 7        | 7        | 7        | 7        |
|-------|-------|---------|---------|----------|----------|----------|----------|----------|
| Order | 2     | 3       | 4       | 5        | 6        | 7        | 8        | 9        |
| Str*  | 7     | 4*8 + 8 | 6*8 + 8 | 10*8 + 8 | 12*8 + 8 | -        | -        | -        |
| 9     | 40    | 56      | 88      | 104      | 14*8 + 8 | 18*8 + 8 | 22*8 + 8 | 24*8 + 8 |
| 11    | 40    | 56      | 88      | 104      | 120      | 152      | 184      | 200      |
| ..... | ..... | .....   | .....   | .....    | .....    | .....    | .....    | .....    |
| 35    | 40    | 56      | 88      | 104      | 120      | 152      | 184      | 200      |

[\*] Ns, Neighborhood Size; Str, Textured Region Size

performance of GLCM texture on mangrove species discrimination is degraded with the growth of the offset (local pattern), especially within the textured region of less than 13 by 13 pixels. This impact becomes weaker with an increase in the textured region size. When it reaches 21 by 21 pixels, the overall accuracy remains stable with an insignificant change (approximately 0.14% drop) from the local pattern.

The performance of GMRF texture, by contrast, is also degraded with the growth of ‘order’ within a textured region of no more than 15 by 15 pixels, but the rate of decline is notably lower (approximately 1%). When the textured region size increases by 15 by 15 pixels, it starts to rise with the growth of the *order*, but the contribution to the separability of mangrove species is still limited (*slope* < 0.01). Therefore, we can conclude that:

- 1) The performance of texture on mangrove species discrimination is sensitive to offset or order when the textured region is small, and it will degrade significantly with the growth of offset or order;
- 2) The declining trend of classification accuracy over offset or order will stabilize if the textured region size grows up to a certain value;
- 3) Using small local patterns rather than larger ones will have a better result, and a local pattern with an offset of 1 for GLCM and an order of 2 for GMRF is suitable for mangrove species classification.

Visually, conclusion 3 can also be obtained from the change in the texture feature images (Fig. 6), which become coarser when the order increases from 2 to 9. However, the mechanisms for presenting rough texture are different between GMRF and GLCM. The spatial autocorrelation between the central pixel and those pixels on the ring becomes weaker when the offset (distance) increases, which makes the GLCM texture coarser. By contrast, GMRF blurs the details by introducing more pixels into the equation formation and parameters estimation of the GMRF model, and the contribution each pixel makes to texture description decreases. A possible reason for the fluctuation and instability of overall accuracy within the small textured region (Fig. 5) is that the number of local patterns is not sufficient to represent a complete texture image of an individual mangrove tree.

### Optimization of Textured Region Size on Mangrove Species Discrimination

The texture region is an area in which texture can be perceived. How its size affects the classification accuracy for mangrove species can be assessed with the help of these data by exchanging axes. Two line graphs of overall accuracy over textured region size with different local patterns can accordingly be drawn, as shown in Fig. 7.

Generally, increasing the textured region size will improve the overall accuracy, which suits both GLCM and GMRF. To show the movement in overall accuracy, we

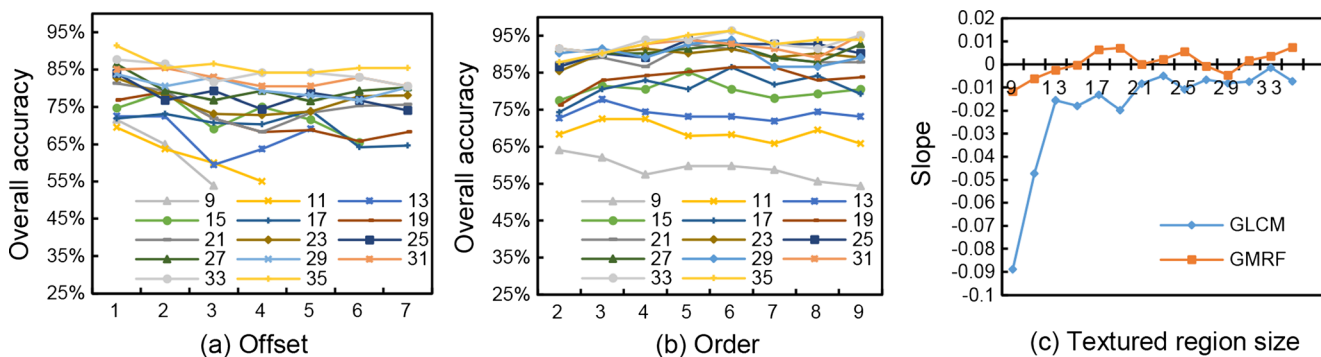


**Fig. 5** The effects of the local pattern extracted by GLCM (a) and GMRF (b) on mangrove species discrimination, and the slope of trend line for the change of overall accuracy at different textured region sizes (c)

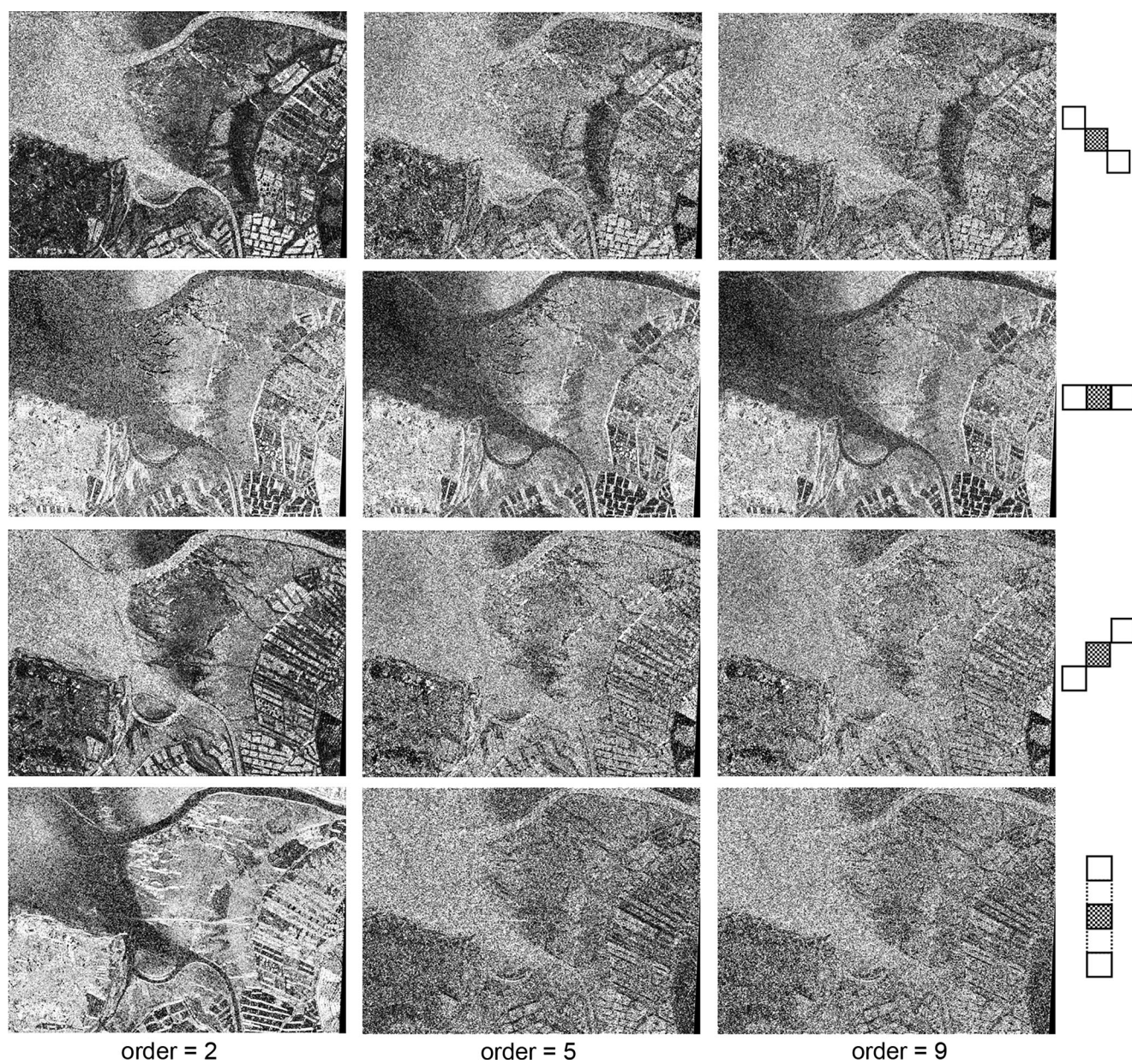


**Fig. 6** Texture images with different local patterns in four dominant directions

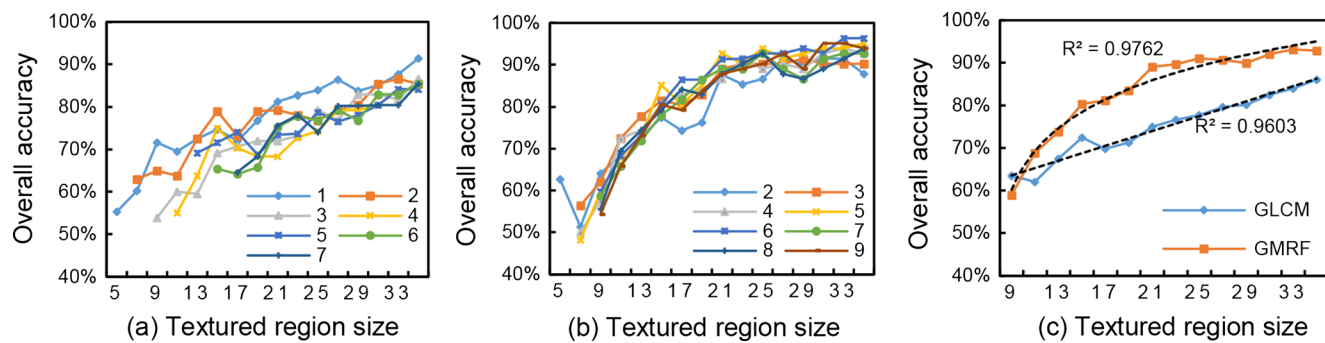


**Fig. 7** The effect of the textured region size of GLCM (a) and GMRF (b), and its averaged effect on mangrove species discrimination (c)

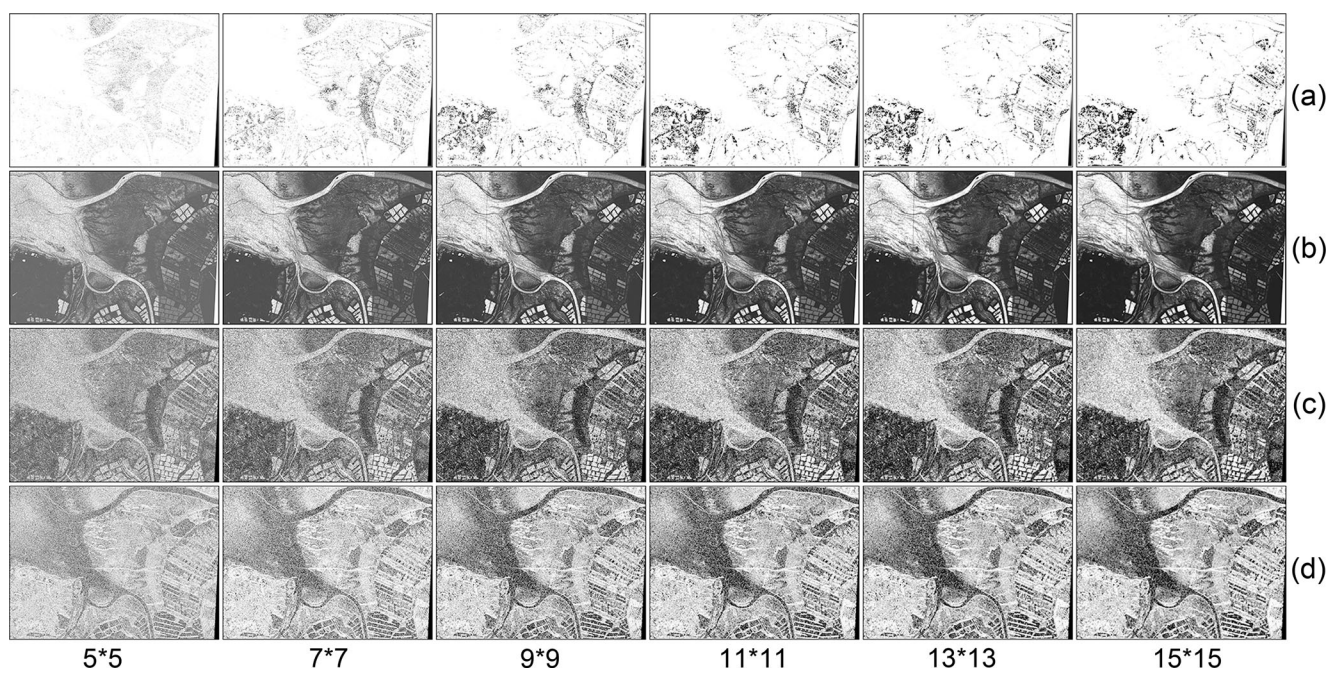


**Fig. 8** **a** Correlation **b** Second moment **c** In 135° direction **d** In 90° direction with different textured region size

averaged the overall accuracy at each size of textured region, generating two new line graphs. The trendlines were then calculated using linear and logarithmic regression with R-squared values of 0.9603 and 0.9762. As shown, the overall accuracy increases approximately linearly when using GLCM and increases approximately logarithmically when using GMRF. For both GLCM and GMRF, the overall accuracy is sensitive to the change of the textured region size at the beginning of its growth, presenting violent fluctuation and sharp increase. This can be explained by the change in the number of valid pixels during the period in which the textured region size increases gradually. To validate this conjecture, the texture features of mangrove forests were extracted with different textured region sizes and partial textural feature images of band five while keeping the local pattern fixed (Fig. 8). As shown, the textural feature images become clearer with the growth of the texture region size, and the magnitude of this change noticeably decreases when the size reaches approximately 13 by

13 pixels. Therefore, we can infer that in textured region size selection, a larger textured region rather than a smaller one can offer better texture information and improve classification accuracy.

Another factor alongside the growth of textured region size is the density of texture information; more pure texture information contained within the textured region will solidify the performance of texture extraction, though further expansion of the textured region increases the risk of the contamination by other classes. Since the newly added information is subordinated to the existing information and statistics as adopted by GLCM to derive texture features, the accuracy increase will not change immediately. The stable peak of the overall accuracy is predicted in the subsequent increase in the textured region size, but as we had to halt the trial due to the time-consuming computing, the question of the optimal textured region size for texture extraction and mangrove species discrimination is still under investigation.

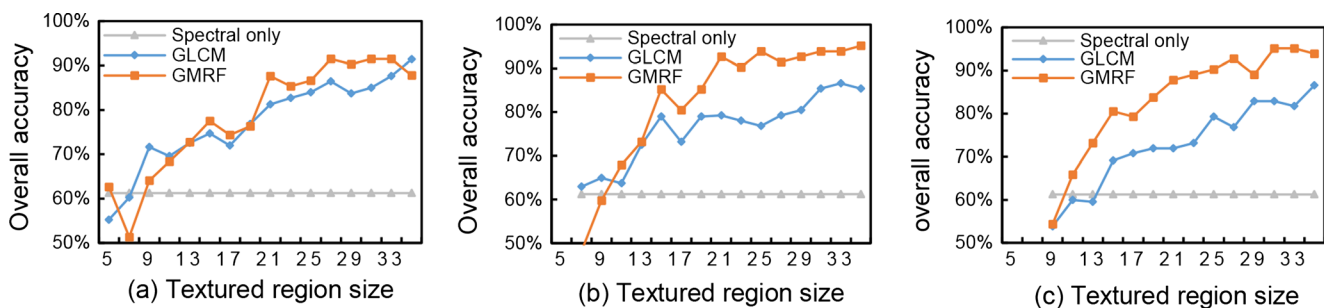


**Fig. 9** Comparison of GLCM, GMRF and spectral features with same size of local pattern at different textured region sizes, **(a)** offset = 1, order = 2; **(b)** offset = 2, order = 5; **(c)** offset = 3; order = 9

## Contribution of Textures to Mangrove Species Discrimination

In terms of contribution of texture to mangrove species discrimination, three aspects, including whether the texture makes a positive contribution, how much contribution it makes and which model between GMRF and GLCM makes more contributions, should be discussed. Since there are multiple orders for an offset using GMRF, the best one is selected for comparison ( $offset = \{1, 2, 3\}$  for GLCM and  $order = \{2, 5, 9\}$  for GMRF) and the discrimination with spectral features alone is also added as the benchmark (Fig. 9).

As shown, texture improves the discrimination accuracy only where the textured region is no less than 11 by 11 pixels. The GMRF texture is more helpful than the GLCM texture where the textured region size exceeds a threshold which varies with the local pattern (13 for local pattern of 3 by 3 pixels, 11 for that of 5 by 5 and 7 by 7 pixels). Under the same conditions, GMRF outperforms GLCM with an overall accuracy improvement of 1.54%, 6.47% and 10.66% on average at a local pattern size of 3 by 3, 5 by 5 and 7 by 7 pixels, respectively.

Furthermore, the textured region size displaying the best accuracy was also selected for both GLCM and GMRF for the purpose of comparison. GLCM reaches its summit at a textured region size of 35 by 35 pixels and an offset of 1, while GMRF peaks at a smaller textured region size (27 by 27 pixels) and an order of 2. The classification of mangrove species (Fig. 10b and Fig. 10c) and confusion matrixes (Table 4) are depicted below, and the classification derived from spectral features only was also added to assess the texture (Fig. 10a).

In terms of the integrity of classification in Fig. 10, the effect of “salt-and-pepper” is reduced after incorporating texture information, and the overall accuracy increases from 61.25% to 91.36% (GLCM) and 91.46% (GMRF). The producer’s accuracy for the six mangrove species is improved as well. In particular, the increase in the producer’s accuracy for AM and AI1 is significant while the increase of KO1 is limited. This effect is due to the intra-class spectral variability in how

**Table 4** Confusion matrices for classification with different kinds of information, (a) spectral only; (b) GLCM texture; (c) GMRF texture ([\*] Uc stands for unclassified, UA stands user’s accuracy (=1-commission error), PA stands for producer’s accuracy (=1-omission error))

|  | AM   | AI1  | AI2  | KO1 | KO2  | AC   | Total | UA(%) |
|--|------|------|------|-----|------|------|-------|-------|
| (a)  |      |      |      |     |      |      |       |       |
| AM   | 5    | 1    | 2    | 2   | 0    | 0    | 10    | 50.0  |
| AI1  | 4    | 10   | 1    | 0   | 0    | 1    | 16    | 62.5  |
| AI2  | 3    | 5    | 8    | 0   | 1    | 4    | 21    | 38.1  |
| KO1  | 3    | 0    | 0    | 17  | 2    | 0    | 22    | 72.3  |
| KO2  | 1    | 0    | 0    | 1   | 9    | 0    | 11    | 81.8  |
| AC   | 0    | 0    | 0    | 0   | 0    | 0    | 0     | 0     |
| Uc*  | 0    | 0    | 0    | 0   | 0    | 2    | 2     | -     |
| Total  | 16   | 16   | 11   | 20  | 12   | 7    | 82    | -     |
| PA(%)  | 31.3 | 62.5 | 72.7 | 85  | 75   | 0    | -     | -     |
| Overall accuracy = 61.2500%; kappa = 0.5213; |      |      |      |     |      |      |       |       |
| (b)  |      |      |      |     |      |      |       |       |
| AM   | 13   | 0    | 0    | 0   | 0    | 0    | 13    | 100   |
| AI1  | 1    | 14   | 0    | 0   | 0    | 0    | 15    | 93.3  |
| AI2  | 1    | 0    | 11   | 0   | 0    | 1    | 13    | 84.6  |
| KO1  | 1    | 0    | 0    | 20  | 2    | 0    | 23    | 87.0  |
| KO2  | 0    | 0    | 0    | 0   | 10   | 0    | 10    | 100   |
| AC   | 0    | 1    | 0    | 0   | 0    | 6    | 7     | 85.7  |
| Uc*  | 0    | 1    | 0    | 0   | 0    | 0    | 1     | -     |
| Total  | 16   | 16   | 11   | 20  | 12   | 7    | 82    | -     |
| PA(%)  | 81.3 | 93.3 | 100  | 100 | 83.3 | 85.7 | -     | -     |
| Overall accuracy = 91.3580%; kappa = 0.8941; |      |      |      |     |      |      |       |       |
| (c)  |      |      |      |     |      |      |       |       |
| AM   | 15   | 0    | 1    | 0   | 1    | 0    | 17    | 88.2  |
| AI1  | 1    | 16   | 0    | 0   | 0    | 0    | 17    | 94.1  |
| AI2  | 0    | 0    | 9    | 0   | 0    | 2    | 11    | 81.8  |
| KO1  | 0    | 0    | 0    | 20  | 1    | 0    | 21    | 95.2  |
| KO2  | 0    | 0    | 1    | 0   | 10   | 0    | 11    | 90.9  |
| AC   | 0    | 0    | 0    | 0   | 0    | 5    | 5     | 100   |
| Uc*  | 0    | 0    | 0    | 0   | 0    | 0    | 0     | -     |
| Total  | 16   | 16   | 11   | 20  | 12   | 7    | 82    | -     |
| PA(%)  | 93.8 | 100  | 81.2 | 100 | 83.3 | 71.4 | -     | -     |
| Overall accuracy = 91.4634%; kappa = 0.8951; |      |      |      |     |      |      |       |       |

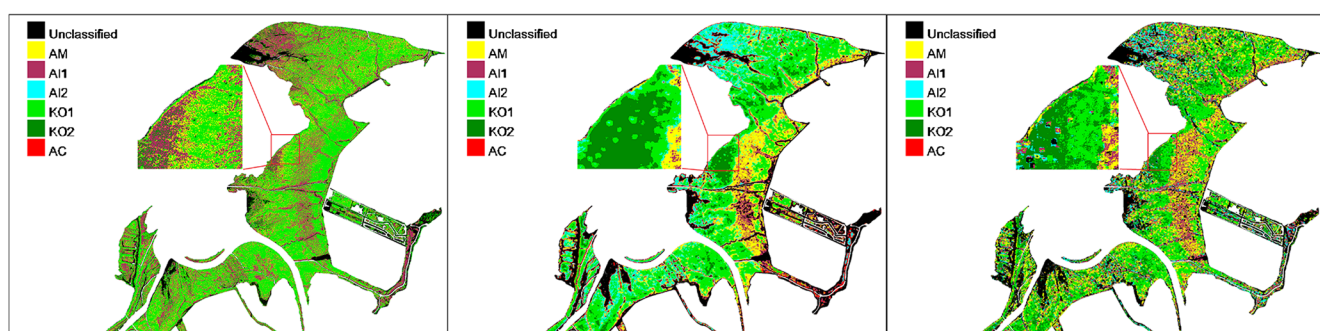
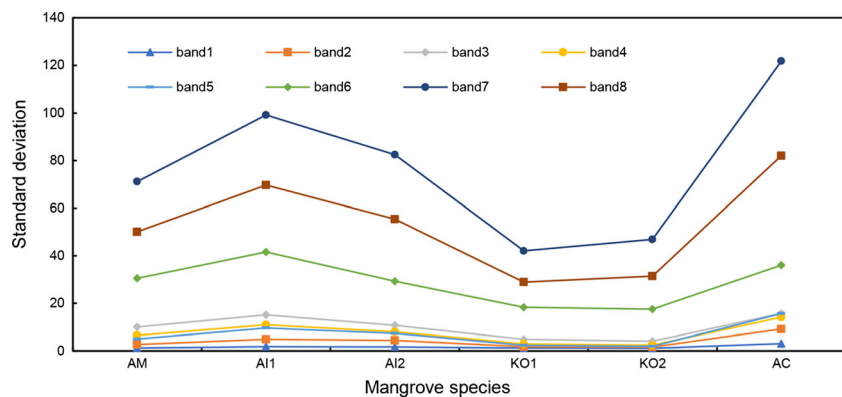


**Fig. 10** Classification with different kinds of information, (a) spectral only; (b) GLCM texture; (c) GMRF texture

**Fig. 11** Standard deviation of 6 mangrove species inter-class



*AM* and *AI1* are distinguished (Fig. 11) and reduces spectral separability (Yu et al. 2006), and can be solved with textures incorporating spatial information. The limited increase of *KO1* is explained by the intra-class spectrum, which does not vary dramatically; a comfortable discrimination can be obtained via the spectral difference from other species. *AC* is a special case which can be recognized only with texture information; the producer's accuracy reaches up to 85.7% and 71.4% with GLCM and GMRF texture information, respectively.

Compared to GLCM texture information incorporation, GMRF texture information seems to be more effective in discriminating *AM* and *AI1* species with a “cluster” characteristic, with an increase of 12.5% and 6.7%, respectively, in the producer's accuracy. By contrast, using GMRF offers an inferior effect on improving the discrimination of *AI2* and *AC*. We searched for insight into the omission samples from the two different methods, and apart from the many samples (marked with dash-line boxes in black) misclassified into the same wrong group using both methods, we found that GLCM is vulnerable to “marginal effect.” The *AI1* samples (marked with solid-line boxes in red in Fig. 12a) with the pixels of exotic classes, such as

water and bare soil, were misclassified into other groups. Additionally, an *AC* sample (marked with solid-line boxes in red in Fig. 12b) was misclassified into the *AI2* group, causing a lower producer's accuracy. However, the figure seems visually reasonable (Fig. 13) with the *AC* sample containing scattered mudflats showing more similarities to the *AI2* samples and slight differences with the rest of the *AC* samples that contained mudflats in a patch. Moreover, fewer testing samples were found in *AI2* and *AC* compared to other species, and whether this was the cause of GMRF's underestimation when discriminating between *AI2* and *AC* species is under investigation. In other words, more testing samples are needed to assess the performance of GLCM and GMRF texture information in producer's accuracy enhancement of *AC*.

In addition to the higher overall accuracy, the advantages of GMRF over GLCM are displayed by the smaller textured region size used to achieve its results (37 versus 25). A smaller textured region not only reduces the problem of “marginal effect,” but also saves considerable time on texture features computing. Finally, we found the “salt-and-pepper” effect of the classification image generated when using GMRF is more notable than that shown when

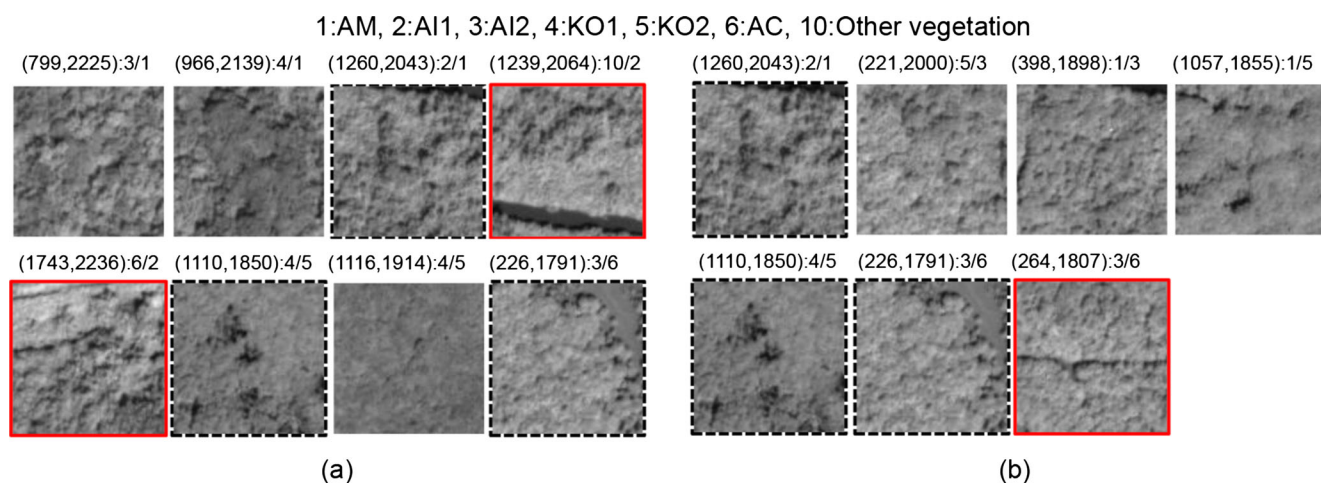


**Fig. 12** Omission samples using GLCM (a) and GMRF (b) with textured region size of 35 by 35 and 27 by 27 pixels (the numbers in parentheses indicate coordinates)

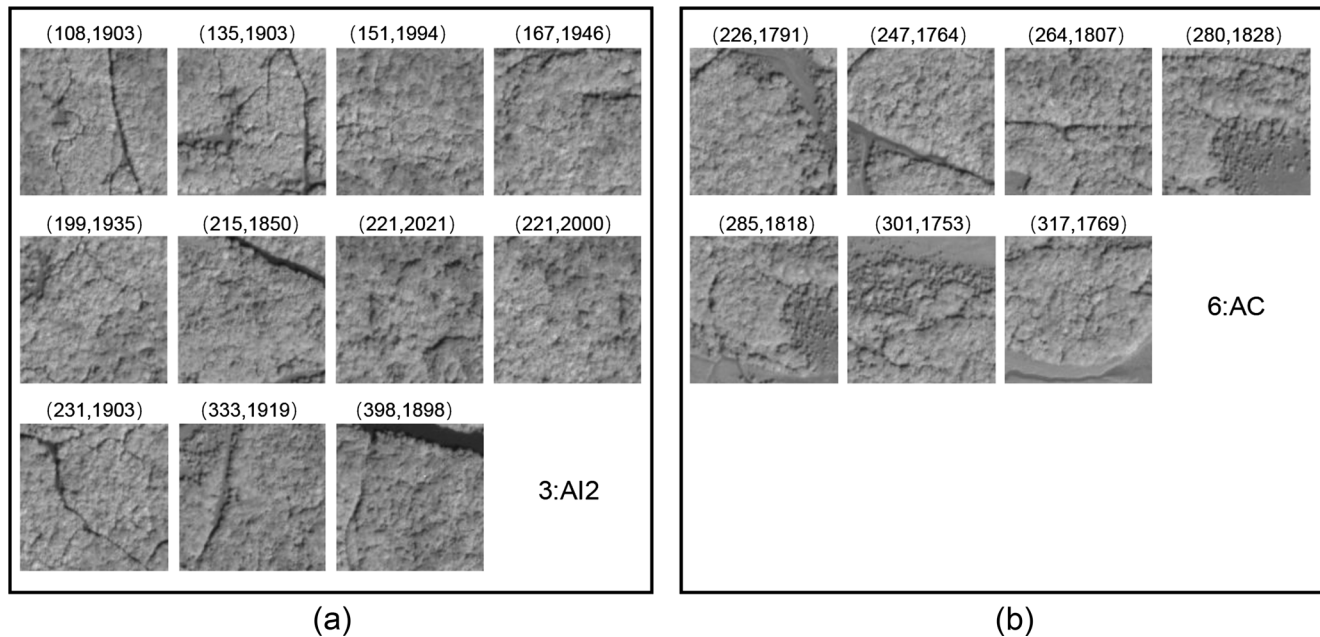


**Fig. 13** The testing samples of AI2 and AC (the numbers in parentheses indicate coordinates)

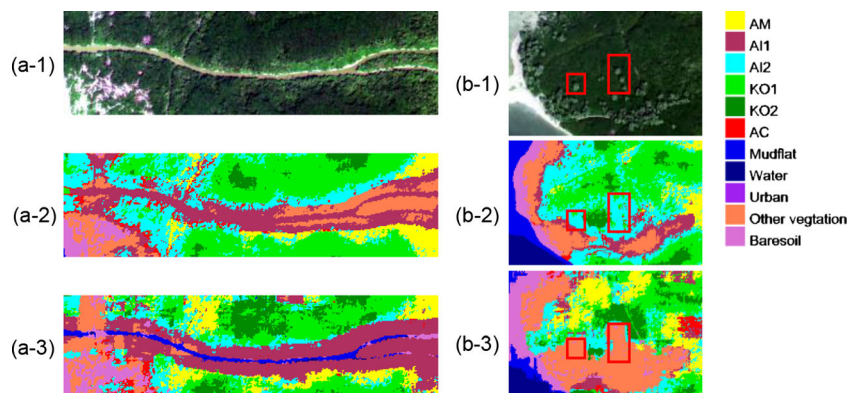
using GLCM. In results generated using GLCM, the characteristic information of an isolated class will be occluded by that of its surrounding class due to its handling of subordination. Conversely, using GMRF, the difference equations the local patterns form are equivalent if the local patterns belong to one class. This indicates that GMRF focuses on the types of local pattern rather than their number. Consequently, the isolated class maintains a powerful influence on texture features and can be distinguished from its surroundings. As a result, GMRF displays a “salt-and-pepper” effect with a higher accuracy. Because of this characteristic, more detailed important information such as a narrow watercourse in mangrove forest (Fig. 14a-1, a-2, a-3) or the scattered plants (Fig. 14b-1, b-2, b-3) can be explored. The watercourses have a significant influence on mangrove seed dispersal and the scattered plants are the suspected invasive species *Sonneratia apetala*.

**Fig. 14** The detailed information was addressed differently by the GLCM and GMRF methods; two cases including a narrow watercourse (**a**) and scattered plants (**b**) were presented with their original images (*a*-1, *b*-1), classification with GLCM texture (*a*-2, *b*-2) and GMRF texture (*a*-3, *b*-3)

## Conclusions

In this paper, the effect of texture derived from GMRF and GLCM on mangrove species discrimination using WV3 imagery was assessed and compared based on the knowledge that texture can be understood through the perspectives of local pattern and textured region size. The main findings of this paper can be summarized in the following points:

- 1) GMRF has a clear advantage over GLCM in mangrove species discrimination when used with the same local pattern sizes (1.54%, 6.47% and 10.66% on average at local pattern sizes of 3 by 3, 5 by 5 and 7 by 7 pixels, respectively), and has a stronger ability to discriminate AM and AI1.
- 2) The overall accuracy was improved from 61.25% to more than 90% with the help of texture, and the AC species was only identifiable using texture.



- 3) Compared to the contribution of local pattern, textured region size plays a major role in the accuracy improvement of mangrove species discrimination. Smaller sizing of the local pattern is preferable for use in deriving the texture of mangrove, while a small region will make the texture invalid.
- 4) GMRF texture shows potential for early warning of mangrove forest invasion due to its ability to detect detailed information with higher accuracy using a smaller size of textured region.

However, this paper has several notable limitations. For instance, limited samples were collected, the field work was limited to a specific area, and visual interpretation rather than primary data was used in most cases. The optimal region size to realize maximum efficiency in texture extraction and mangrove species discrimination is still under investigation, and while the edge effect brought by large textured regions does not invariably cause low accuracy, it may lead to an optimistic accuracy (Fern and Warner 2002) as well.

**Acknowledgments** This study was jointly supported by The Research Grants Council (RGC) General Research Fund (CUHK 14635916), the Major Special Project—the China High-resolution Earth Observation System (Grant number 11-Y20A40-9002-15/17), National Natural Science Foundation of China (41401370), Guangdong Key Laboratory of Ocean Remote Sensing (South China Sea Institute of Oceanology Chinese Academy of Sciences) (2017B030301005-LORS1801), and National Key Research and Development Program of China (Project Ref. No. 2016YFB0501501). The authors would like to thank the editor and two anonymous reviewers for their critical comments and suggestions to improve the original manuscript.

## References

- AFCD (2015) Local mangrove species. Agriculture. Fisheries and Conservation Department (AFCD), Hong Kong
- Amari S, Wu S (1999) Improving support vector machine classifiers by modifying kernel functions. *Neural Networks* 12:783–789
- Asadzadeh S, de Souza Filho CR (2016) Investigating the capability of WorldView-3 hyperspectral data for direct hydrocarbon detection. *Remote Sensing of Environment* 173:162–173
- Bharati MH, Liu JJ, MacGregor JF (2004) Image texture analysis: methods and comparisons. *Chemometrics and Intelligent Laboratory Systems* 72:57–71
- Boser BE, Guyon IM, Vapnik VN (1992) A training algorithm for optimal margin classifiers. p. 144–152. Proceedings of the fifth annual workshop on computational learning theory. ACM
- Cao T, Tokushima H, Noguchi Y (2006) Texture analysis using Gaussian Markov random fields. *Reports of the Faculty of Science and Engineering, Saga University* 35:1–10
- Çesmeli E, Wang D (2001) Texture segmentation using Gaussian-Markov random fields and neural oscillator networks. *IEEE Transactions on Neural Networks* 12:394–404
- Chang C-C, Lin C-J (2011) LIBSVM: a library for support vector machines. *ACM Trans Intell Syst Technol* 2:1–27
- Chellappa R, Chatterjee S (1985) Classification of textures using Gaussian Markov random fields. *IEEE Transactions on Acoustic Speech and Signal Processing* 33:959–963
- Chen C-C, Huang C-L (1993) Markov random fields for texture classification. *Pattern Recognition Letters* 14:907–914
- Cohen J (1960) A coefficient of agreement for nominal scales. *Educational and Psychological Measurement* 20:37–46
- Cohen FS, Fan Z, Patel MA (1991a) Classification of rotated and scaled textured images using Gaussian Markov random field models. *IEEE Transactions on Pattern Analysis and Machine Intelligence* 13:192–202
- Cohen FS, Zhigang F, Attali S (1991b) Automated inspection of textile fabrics using textural models. *IEEE Transaction on Pattern Analysis and Machine Intelligence* 13:803–808
- Congalton RG (1983) Assessing landsat classification accuracy using discrete multivariate analysis statistical techniques. *Photogrammetric engineering and remote sensing* 49(12): 1671–1678
- Cortes C, Vapnik V (1995) Support-vector networks. *Machine learning* 20:273–297
- Dahdouh-Guebas F, Van Hiel E, Chan JCW, Jayatissa LP, Koedam N (2004) Qualitative distinction of congeneric and introgressive mangrove species in mixed patchy forest assemblages using high spatial resolution remotely sensed imagery (IKONOS). *Systematics and Biodiversity* 2:113–119
- Ellison A, Farnsworth E, Moore G (2010) *Pelliciera rhizophorae*. The IUCN red list of threatened species 2010: e.T178833A7621318. <https://doi.org/10.2305/IUCN.UK.2010-2.RLTS.T178833A7621318.en>
- Feng Q, Liu J, Gong J (2015) UAV remote sensing for urban vegetation mapping using random Forest and texture analysis. *Remote Sensing* 7:1074
- Fern CJ, Warner TA (2002) Scale and texture in digital image classification. *Photogrammetric Engineering & Remote Sensing* 68:51–63
- Globe D (2014) Satellite information-WorldView-3. Available at [https://www.spaceimagingme.com/downloads/sensors/datasheets/DG\\_WorldView3\\_DS\\_2014.pdf](https://www.spaceimagingme.com/downloads/sensors/datasheets/DG_WorldView3_DS_2014.pdf). Accessed 7 Dec 2016
- Gonzalez RC, Woods RE (1992) *Digital Image Processing*. Addison-Wesley Longman Publishing Co., Inc, Boston.
- Hammersley JM, Clifford PE (1971) Markov random fields on finite graphs and lattices. Unpublished. Available at <http://www.statslab.cam.ac.uk/~grg/books/hammfest/hamm-cliff.pdf>. Accessed 7 Dec 2016
- Haralick RM (1979) Statistical and structural approaches to texture. *Proceedings of the IEEE* 67:786–804
- Haralick RM, Shanmugam KS (1974) Combined spectral and spatial processing of ERTS imagery data. *Remote Sensing of Environment* 3:3–13
- Haralick RM, Shanmugam K, Dinstein IH (1973) Textural features for image classification. *IEEE Transactions on Systems Man and Cybernetics* 3:610–621
- Hawkins JK (1970) Textural properties for pattern recognition. *Picture processing and psychopictorics*. Academic Press, New York. pp 347–370
- Heumann BW (2011) An object-based classification of mangroves using a hybrid decision tree—support vector machine approach. *Remote Sensing* 3:2440–2460
- Hsu C-W, Chang C-C, Lin C-J (2003) A practical guide to support vector classification. Technical report. Available at <https://www.csie.ntu.edu.tw/~cjlin/papers/guide/guide.pdf>. Accessed 10 Dec 2016
- Huang X, Zhang L (2013) An SVM ensemble approach combining spectral, structural, and semantic features for the classification of high-resolution remotely sensed imagery. *IEEE Transactions on Geoscience and Remote Sensing* 51:257–272

- Huang C, Davis L, Townshend J (2002) An assessment of support vector machines for land cover classification. *International Journal of Remote Sensing* 23:725–749
- Huang X, Zhang L, Wang L (2009) Evaluation of morphological texture features for mangrove forest mapping and species discrimination using multispectral IKONOS imagery. *IEEE Geoscience and Remote Sensing Letters* 6:393–397
- Jia M, Wang Z, Li L, Song K, Ren C, Liu B, Mao D (2014) Mapping China's mangroves based on an object-oriented classification of Landsat imagery. *Wetlands* 34:277–283
- Keerthi SS, Lin C-J (2003) Asymptotic behaviors of support vector machines with Gaussian kernel. *Neural computation* 15:1667–1689
- Kruse FA, Perry SL (2013) Mineral mapping using simulated Worldview-3 short-wave-infrared imagery. *Remote Sensing* 5:2688–2703
- Li D, Ke Y, Gong H, Li X (2015) Object-based urban tree species classification using bi-temporal WorldView-2 and WorldView-3 images. *Remote Sensing* 7:16917–16937
- Li SZ (2009) Markov random field modeling in image analysis. Springer, London
- Mather P, Tso B (2003) Classification methods for remotely sensed data. CRC Press, Boca Raton
- Melgani F, Bruzzone L (2004) Classification of hyperspectral remote sensing images with support vector machines. *IEEE Transactions on Geoscience and Remote Sensing* 42:1778–1790
- Mountrakis G, Im J, Ogole C (2011) Support vector machines in remote sensing: a review. *ISPRS Journal of Photogrammetry and Remote Sensing* 66:247–259
- Myint SW, Giri CP, Wang L, Zhu Z, Gillette SC (2008) Identifying mangrove species and their surrounding land use and land cover classes using an object-oriented approach with a lacunarity spatial measure. *GIScience & Remote Sensing* 45:188–208
- NC (2005) Mangrove - the Nature conservancy. In: How we work. The Nature Conservancy (NC), Arlington
- Neukermans G, Dahdouh-Guebas F, Kairo JG, Koedam N (2008) Mangrove species and stand mapping in Gazi Bay (Kenya) using Quickbird satellite imagery. *Journal of Spatial Science* 53:75–86
- Peng L (2003) The characteristics of mangrove wetlands and some ecological Engineering questions in China [J]. *Engineering Science* 6:4
- Pham M-T, Mercier G, Regniers O, Michel J (2016) Texture retrieval from VHR optical remote sensed images using the local Extrema descriptor with application to vineyard parcel detection. *Remote Sensing* 8:368
- Qin P, Wong YS, Tam NFY (2000) Emergy evaluation of Mai Po mangrove marshes. *Ecological Engineering* 16:271–280
- Ren H, Lu H, Shen W, Huang C, Guo Q, Za L, Jian S (2009) Sonneratia Apetala Buch. Ham in the mangrove ecosystems of China: an invasive species or restoration species? *Ecological Engineering* 35: 1243–1248
- Roli F, Fumera G (2001) Support vector machines for remote sensing image classification. *Europto remote sensing. International Society for Optics and Photonics* 4170:160–166
- Sulong I, Mohd-Lokman H, Mohd-Tarmizi K, Ismail A (2002) Mangrove mapping using Landsat imagery and aerial photographs: Kemaman District, Terengganu, Malaysia. *Environment, Development and Sustainability* 4:135–152
- Tuceryan M, Jain AK (1993) Texture analysis. *Handbook of pattern recognition and computer vision* 2:207–248
- Verheyden A, Dahdouh-Guebas F, Thomaes K, De Genst W, Hettiarachchi S, Koedam N (2002) High-resolution vegetation data for mangrove research as obtained from aerial photography. *Environment, Development and Sustainability* 4:113–133
- Wang L, Sousa W, Gong P (2004a) Integration of object-based and pixel-based classification for mapping mangroves with IKONOS imagery. *International Journal of Remote Sensing* 25:5655–5668
- Wang L, Sousa WP, Gong P, Biging GS (2004b) Comparison of IKONOS and QuickBird images for mapping mangrove species on the Caribbean coast of Panama. *Remote Sensing of Environment* 91:432–440
- Wang T, Zhang H, Lin H, Fang C (2015) Textural-spectral feature-based species classification of mangroves in Mai Po Nature reserve from Worldview-3 imagery. *Remote Sensing* 8:24
- Wilkie ML, Fortuna S (2003) Status and trends in mangrove area extent worldwide. FAO, F. R. Division, Rome
- Wong FKK, Fung T (2014) Combining EO-1 Hyperion and Envisat ASAR data for mangrove species classification in Mai Po Ramsar site, Hong Kong. *International Journal of Remote Sensing* 35:7828–7856
- Xia GS, He C, Yu L, Sun H (2006) Urban extraction from SAR images using local statistical characteristics and gaussian markov random field mod. p. 1. 2006 8th international Conference on Signal Processing
- Yu Q, Gong P, Clinton N, Biging G, Kelly M, Schirokauer D (2006) Object-based detailed vegetation classification with airborne high spatial resolution remote sensing imagery. *Photogrammetric Engineering & Remote Sensing* 72(7):799–811
- Zhang H, Lin H, Li Y, Zhang Y (2013) Feature extraction for high-resolution imagery based on human visual perception. *International Journal of Remote Sensing* 34:1146–1163
- Zheng GJ, Lam MHW, Lam PKS, Richardson BJ, Man BKW, Li AMY (2000) Concentrations of persistent organic pollutants in surface sediments of the mudflat and mangroves at Mai Po marshes Nature reserve, Hong Kong. *Marine Pollution Bulletin* 40:1210–1214